Electrokinetics in nanochannels
Part I. Electric double layer overlap and channel-to-well equilibrium

Fabio Baldessari

Department of Mechanical Engineering, Stanford University, Stanford, CA 94305, USA

ARTICLE INFO

ABSTRACT

In this paper a new model is described for calculating the electric potential field in a long, thin nanochannel with overlapped electric double layers. Electrolyte concentration in the nanochannel is predicted self-consistently via equilibrium between ionic solution in the wells and within the nanochannel. Differently than published models that require detailed iterative numerical solutions of coupled differential equations, the framework presented here is self-consistent and predictions are obtained solving a simple one-dimensional integral. The derivation clearly shows that the electric potential field depends on three new parameters: the ratio of ion density in the channel to ion density in the wells; the ratio of free-charge density to bulk ion density within the channel; and a modified Debye–Hückel thickness, which is the relevant scale for shielding of surface net charge. For completeness, three wall–surface boundary conditions are analyzed: specified zeta-potential; specified surface net charge density; and charge regulation. Predictions of experimentally observable quantities based on the model proposed here, such as depth-averaged electroosmotic flow and net ionic current, are significantly different than results from previous overlapped electric double layer models. In this first paper of a series of two, predictions are presented where channel depth is varied at constant well concentration. Results show that under conditions of electric double layer overlap, electroosmosis contributes only a small fraction of the net ionic current, and that most of the measurable current is due to ionic conduction in conditions of increased counterion density in the nanochannel. In the second of this two-paper series, predictions are presented where well-concentration is varied and the channel depth is held constant, and the model described here is employed to study the dependence of ion mobility on ionic strength, and compare predictions to measurements of ionic current as a function of channel depth and ion density.

© 2008 Elsevier Inc. All rights reserved.

1. Introduction

Recent advances in nanofabrication have allowed for detailed experimental investigations of electrokinetic fluid flow in long, thin channels with characteristic dimensions in the range of tens of nanometers (nanochannels) [1–5]. At this length scale, electric double layers (EDLs) at the wall/electrolyte interface strongly influence axial ion transport rates, total ionic current (both advective and electromigration current), and bulk flow. EDLs are characterized by the presence of high concentrations of excess counter charges required to shield surface net charge. For infinitely long channels with depths on the order of or smaller than the EDL length scale, wall EDLs can interact strongly and there is net free charge throughout the channel cross section. For finite length channels, connected to wells, the charge distribution is ultimately determined by at least a quasi-equilibrium balance between wall

surface charge (and associated surface chemistry) and the ion densities in end-channel wells.

Various models have been proposed to treat the ionic equilibria and electrokinetic transport characteristics of nanochannels with finite and overlapped EDLs. Table 1 summarizes published continuum models describing liquid flow and ionic concentration equilibrium dynamics in the presence of EDL overlap. The ten models reflect different assumptions regarding the governing physical mechanisms, which are imposed (nearly always) through the choice in boundary conditions for the ionic concentrations and electric potential field, and the choice of using constraints of electroneutrality (local balance between positive and negative charge) and of net neutrality (cross-section-area-averaged balance of charge including wall charge).

All of the models are based on descriptions of an electrolyte in thermodynamic equilibrium near a charged surface, and rely on the Poisson equation for the electrostatic potential, the Boltzmann distribution for diffuse electrolyte ions, and the Stokes equations for unidirectional liquid flow in the presence of an electrical body

E-mail address: fabio.baldessari@gmail.com.

Table 1

List of published theoretical models for predicting electrostatic potential field and ion density distribution, in long, thin channels, in conditions where the EDLs overlap (weak to strong overlap are included). A number of these works also include a treatment of electrokinetic flows. Models are classified based on their defining assumptions. Models are listed in the chronological order they were published

Models for symmetric (top/bottom surfaces) channels (in chronological order)	Open/ closed system	Debye–Hückel approx.	Boundary condition on ionic concentrations				Wall boundary condition on electric potential			Net neutrality and electroneutrality conditions			Ionic strength dependence of ionic mobility
			Specified centerline value	Specified wall value	Water dissociation EQL	EQL between wells and channel	Specified zeta-potential	Specified surface charge density	Chemical EQL	Channel cross-section is net neutral	ENT in the wells	Global net neutrality	
Burgreen and Nakache [6–8,27]	Open		X				X						
Qu and Li [14,15]	Open	X			X			X					
Conlisk et al. [19]	Open			X			X			X			
Zheng et al. [20,21]	Closed					X	X			X	X		
Stein et al. [1,9]	Open		X					X					
Van der Heyden et al. [10]	Open		X				X	X	X				
Kwak and Hasselbrink [17,18]	Open			X		X		X[a]		X			
Schoch et al. [4,5]	Open		X									X	
Tessier and Slater [22]	Closed, no wells							X		X			
Baldessari (current work)	Closed					X	X	X	X			X	X

Note. ENT = electroneutrality; conc. = concentration; EQL = equilibrium.

[a] Time dependent calculations where surface charge is turned "ON" at $t = 0$.

force. Differences among model predictions stem from assumptions of the ion density and/or potential at the channel surface and the channel centerline.

For slit channels (infinitely long, thin channels with rectangular cross-section), Burgreen and Nakache [6] were the first to model the presence of thick EDL and its effect on advection and conduction of electrolyte ions. Their model includes treatment of the (equilibrium) transverse electric potential distribution, its implications on electroosmotic flow, and on ionic current and streaming potential measurements. Burgreen and Nakache assume the following: ion concentration in the bulk can be specified independently of the electric potential (assumed small at the center of the channel); and potential at the shear plane (zeta potential) is a known, fixed value. Their predictions are accurate provided the degree of overlap is small (so called weakly interacting EDLs). Other investigators proposed similar models with minor variations [7,8].

In the last few years, some studies have extended the theoretical framework of Burgreen and Nakache and compared predictions to electrokinetic transport measurements. Stein et al. [1] modified the boundary conditions of the Burgreen and Nakache model to make predictions for specified (and fixed) surface net charge density at the channel walls, instead of specified zeta potential. This choice of boundary condition can affect significantly the electric potential distribution in the channel (and therefore electroosmotic flow and ionic current). Stein et al. used the value of surface net charge density as fitting parameter when comparing to measured ionic current in 70–1015 nm deep silica channels with aqueous potassium chloride (KCl) solutions and 10 mM TRIS salt. They fit observed trends in electric conductance at high and low salt concentrations and constant channel height, using surface net charge density values between -45 and -68 mC/m^2 [9]. Van der Heyden et al. [10] measured streaming currents in 70–1147 nm deep silica channels as a function of applied pressure with aqueous solutions of KCl and TRIS. They observed that streaming current increases as KCl concentration is reduced from 1 M to 1 mM, but below 1 mM conductance saturates to (approximately) a constant value. To model these experiments, they assume that the ionic concentration in the bulk of the nanochannel can be specified independently of other parameters (similarly to Burgreen and Nakache), but they proposed a different (third) choice for the wall boundary condi-

tion on the electric potential distribution: a chemical equilibrium deprotonation reaction of the silanol groups on the silica surface (specifically a boundary condition known as "charge regulation" (CR)) [11–13]. A common deduction made by all these investigators is that, in conditions of thick and overlapped EDLs advective current (bulk ionic motion due to electroosmotic flow) is a significant fraction of total ionic current in the channel. In the calculations presented here it is found in fact that this contribution is never dominant.

Other investigations focused on studying the effects of surface equilibrium reactions to describe local free charge accumulation, and its effects on measurements of conductance. Recently, Qu and Li [14], and Ren et al. [15], proposed a 1D model for overlapped EDLs in infinitely long, thin channels valid for low values of zeta potential (the Debye–Hückle approximation). As a wall boundary condition, they use the site-dissociation model of Healy and White [16] which predicts wall charge based on the pH-dependent surface condensation reaction of hydroxyl or hydronium ions. In this approach, a net free-charge develops because loss of hydroxyl (or hydronium) ions to the surface is only in part countered by dissociation of water molecules. The differences between their predictions and classical predictions assuming Boltzmann equilibrium are large when EDLs are highly overlapped. They argue that applying Boltzmann equilibrium directly is incorrect because it assumes that diffuse ion composition is independent of surface ions. The Qu and Li model neglects the dynamics due to end-effects and the presence of wells; it is valid only for infinitely long thin channels. In reality transport of ions to and from relatively large channel wells eventually establishes Boltzmann distribution type equilibrium between the channel wall and wells. Thus, the behavior found by Qu and Li is descriptive of an intermediate state toward final equilibrium, as verified by detailed time dependent calculations of Kwak and Hasselbrink [17], and Kang and Suh [18], who solve the transient problem starting at the instant when a specified surface net charge density is instantaneously imposed on the nanochannel wall. These calculations show that the final equilibrium state is well described by Boltzmann distributions.

Schoch et al. [4,5] also observed trends of measured conductance for varying electrolyte concentration similar to Stein et al. and van der Heyden et al. Their model is based on linear superposition of the expected bulk conductivity (proportional to the sum

of the product of concentration and mobility for all ions), and a scaling estimate of the contribution to conductance due to the excess counterions in solution inside the nanochannel. To estimate the density of counterions, they impose net neutrality (which is here defined as a net zero sum of the area average charge density including wall charge) for a specified surface charge density. Schoch et al. use this *ad hoc* description, and use the surface net charge density as a fitting parameter to explain trends in measured conductance. They find that a surface charge density of -53 mC/m^2 fits experimental data.

In a series of three publications, Conlisk et al. [19–21] developed models where ionic concentrations at the wall (instead of at the midpoint) are either specified, or determined from channel-to-well equilibrium considerations. When the system is open (infinitely long, slit channel) Conlisk et al. [19] assume that the ion concentrations at the wall are known and that the zeta potential is specified. When the channel is connected to large wells at each end (closed system), Conlisk et al. [20,21] model ionic concentrations inside the nanochannel coupled to concentrations in wells via the Nernst equations. The channel-to-well fluxes are approximated using a one-dimensional flux balance between the depth-averaged concentrations in the nanochannel and the (large) well. They apply net neutrality at each cross section within the nanochannel, and independently apply electroneutrality to the walls and content of wells. Further detailed comments on this issue will be made in Section 2.1 where an equation is derived for the self-consistent coupling of ionic concentrations in the wells and the nanochannel. For now, note that the Conlisk et al. approach requires intensive, iterative, numerical solutions of the constrained boundary value problem for the coupled Poisson (differential) equation for the electrostatic potential, and the Nernst (differential) equations for ionic concentration fields. As mentioned above, in their model the constraints are net neutrality at each cross-section and (separately) electroneutrality in the wells.

Finally, Tessier and Slater [22] present a model to describe the distribution of ions confined between charged surfaces for closed long, thin channels. They specify surface net charge density, and adopt net neutrality at each cross-section of the channel. They show that a closed system is equivalent to the traditional treatment of an open system provided that an effective length scale is introduced in place of the Debye length: the Debye length divided by the geometric mean of the normalized densities of counter and co-ions at the center of the channel.

In this paper, a new theoretical framework is proposed to accurately describe liquid flow and ion transport in nanochannels in conditions of EDL overlap. Two specific modifications are introduced to the existing theories relevant to EDL overlap: (1) how to determine self-consistently the transverse electric potential distribution and the ionic concentrations in a nanochannel in equilibrium with end-channel wells; and (2) how to include the effect of local ionic strength on ion mobility. The first modification above assumes that Boltzmann equilibrium is established between the channel and the wells. This idea is employed to develop a model that allows univocal determination of the two coupled variables in the system: electric potential distribution and ionic concentrations (ion densities).

In the sections that follow, first a derivation is given of the theoretical model, including the results of assuming each of three commonly used boundary conditions for electric potential (specified zeta potential, specified surface charge density, or charge regulation), and of including ionic mobility dependence on ionic strength and pH. Formulations of the electroosmotic flow and net ionic current equations are also presented which are consistent with the electric potential model derived here. Finally, the results presented here describe how one might predict nanochannel

behavior given microchannel measurements of electroosmotic mobility.

2. Theoretical formulation

2.1. Distribution of ions ($n_i(\mathbf{r})$) and free-charge ($\rho_E(\mathbf{r})$)

Consider a nanochannel with dielectric, impermeable walls and a native surface charge as shown schematically in Fig. 1. The channel is bounded by two relatively large electrolyte wells at either end. At equilibrium gradients in the electrochemical potential ($\bar{\mu}_i$) of each species i are zero:

$$\nabla \bar{\mu}_i(\mathbf{r}) = \nabla \big[k_B T \ln n_i(\mathbf{r}) + z_i e \psi(\mathbf{r}) \big] = 0, \tag{1}$$

where $\psi(\mathbf{r})$ is the electric potential in the diffuse charge regions, e is the electron charge, z_i ion valence, $k_B T$ is the thermal energy, and $\mathbf{r}$ is the position vector. Denote the ion number density and the electric potential in the middle of a symmetric channel as $n_i(\mathbf{d}) = n_i^c$ and $\psi(\mathbf{d}) = \psi_c$, where the position vector $\mathbf{d}$ indicates the midplane. The ionic concentration profile ($n_i(\mathbf{r})$) valid for the three dimensional space which includes the inside of the nanochannel and its connecting wells is then the Boltzmann distribution given by [23]

$$n_i(\mathbf{r}) = n_i^c \exp\left(-\frac{e z_i}{k_B T} \big(\psi(\mathbf{r}) - \psi_c \big) \right). \tag{2}$$

The centerline ion concentration (n_i^c) in the nanochannel is unknown at this stage. Solving for n_i^c requires treatment of the equilibrium between ions in the channel and the ions in the end-channel electrolyte wells.

In the absence of applied electric fields, the equilibrium concentration in the nanochannel may differ from that of the wells since electric potentials in the channel may be different than that of the well (i.e., when we have significant double layer overlap). Satisfying $\nabla \bar{\mu}_i = 0$ along the axial channel direction allows to write an equilibrium condition between the ion concentration in the wells (n_i^{well}) and the ion concentration at the centerline of the nanochannel

$$n_i^c = n_i^{well} \exp\left(-\frac{e z_i}{k_B T} \psi_c \right), \tag{3}$$

where it is assumed $\psi_{well} = 0$ as reference electric potential with respect to which all other (wall charge related) electric potentials are measured. Substitution of Eq. (3) into (2) yields an expression for ion distribution in long thin channels

$$n_i(\mathbf{r}) = n_i^{well} \exp\left(-\frac{e z_i}{k_B T} \psi_c \right) \exp\left(-\frac{e z_i}{k_B T} \big(\psi(\mathbf{r}) - \psi_c \big) \right). \tag{4}$$

Choosing to write the ion distribution function as shown in (4) instead of the more compact form

$$n_i(\mathbf{r}) = n_i^{well} \exp\left(-e z_i \psi(\mathbf{r}) / k_B T \right)$$

serves as reminder that a self-consistent solution of $\psi(\mathbf{r})$ requires knowledge of ψ_c which is non-zero and determined by the boundary conditions at the walls, as will be seen in detail in the next section. Given Eq. (4), the distribution of free charge in the electrolyte is given by

$$\rho_E(\mathbf{r}) = \sum_i z_i e n_i(\mathbf{r}) = \sum_i z_i e n_i^c \exp\left(-\frac{e z_i}{k_B T} \big(\psi(\mathbf{r}) - \psi_c \big) \right)$$

$$= \sum_i z_i e n_i^{well} \exp\left(-\frac{e z_i}{k_B T} \psi_c \right) \exp\left(-\frac{e z_i}{k_B T} \big(\psi(\mathbf{r}) - \psi_c \big) \right). \tag{5}$$

To the best of the author's knowledge, this is the first time that explicit functions of the centerline electric potential have been
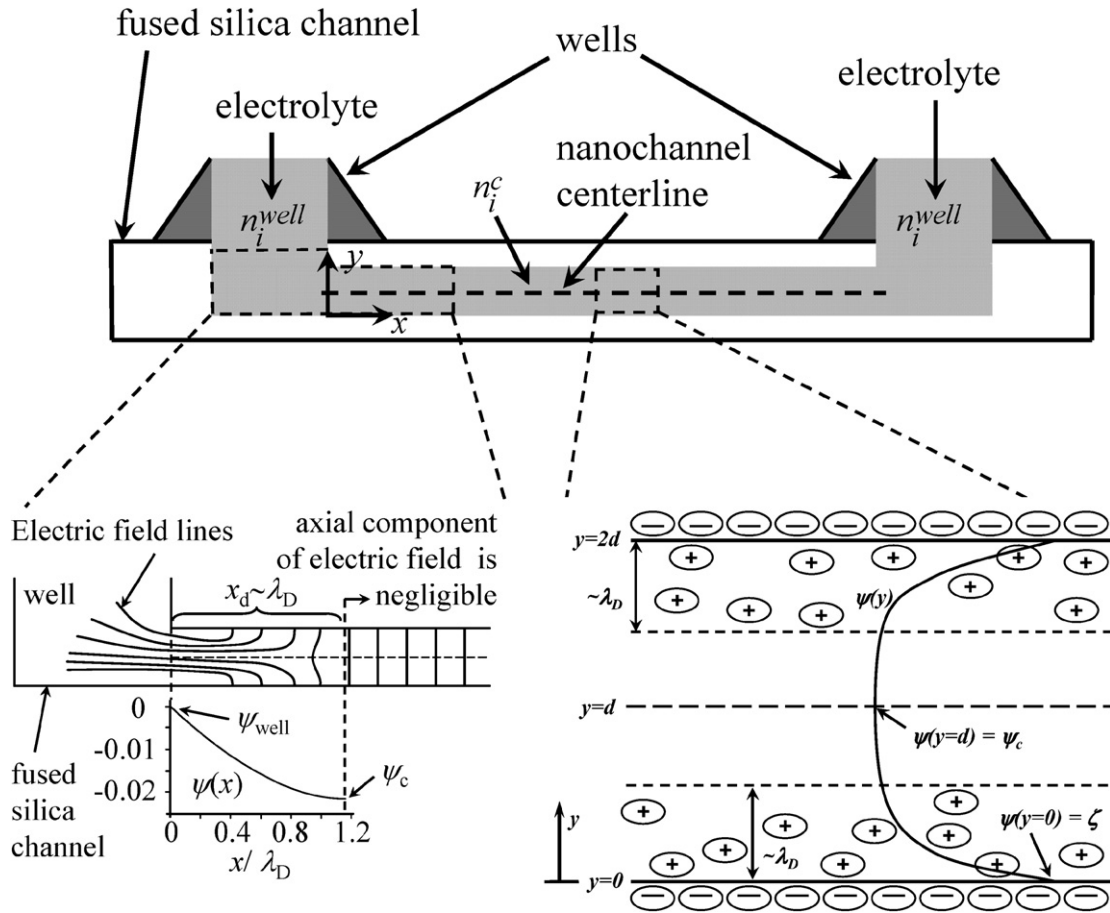
Fig. 1. Schematic of a long, thin nanochannel connected to wells at the ends. Also shown (bottom left) is a schematic of the idealized electric field lines at the transition region between the well and the nanochannel. At the bottom right a schematic is shown of idealized electric double-layers (free-charge) in contact with a charged flat wall (away from the ends of the nanochannel).

used to model self-consistently the ionic concentration inside the nanochannel via a condition of equilibrium between the solutions in the wells and inside a long, thin nanochannel. For example, models based on the work by Burgreen and Nakache [6] assume that the exponential factor in Eq. (3) is unity: i.e., ion densities are specified independently of ψ_c. Conlisk et al. [20,21] also proposed to adopt equilibrium between the wells and the channel. They postulate that the cross-sectional area-averaged electrochemical potential is uniform along the channel length, and equal to the electrochemical potential in the well, and they derive an area-averaged ion density form of Eq. (4). However, they then impose a net neutrality constraint at the channel cross section (including channel wall net charge), and a separate, independent electroneutrality constraint for the electrolyte in the wells. These are part of a single net neutrality constraint for the entire system, and, strictly speaking, should not be imposed separately (see Appendix A). Further, Conlisk et al. eliminate the explicit dependence of ion density on ψ_c, by expressing electroneutrality and net neutrality in terms of concentration ratios, obtained dividing Eq. (4) by the ion density of the most populous species present in solution. The formulation that results from the construct of Conlisk et al. requires iterative solution of non-linear, coupled differential equations with integral constraints. Equations (4) and (5) are in fact new and express the fact that ionic concentrations inside the nanochannel cannot in general be specified independently of ψ_c or independently of the conditions at the sample well. More importantly, these equations embody the explicit dependence on just one variable, ψ_c. This is one of two main modifications, improvements present in the formulation in this paper relative to past work.

2.2. The potential distribution in a wide, shallow channel ($\psi(y)$)

In this section, the discussion is focused on the potential field in a wide, shallow nano-scale channel of the type typically created using planar microfabrication methods [1–3,24–29]. Define y as the transverse coordinate, as in Fig. 1. Assume for now that end-effects due to axial gradients in the potential are confined to small regions near the entrances to the channel, and can be neglected when studying the potential distribution across the channel depth. (This assumption is justified in detail in Appendix B.) The transverse potential distribution (between the top and bottom walls) is obtained solving the Poisson equation subject to the condition of symmetry at the center (here assume that the channel walls are identical), and a second boundary condition at one of the walls. From the one-dimensional (1D) Poisson equation for the electric potential within the double-layer [23]

$$\frac{d^2\psi}{dy^2} = -\frac{1}{\varepsilon} \sum_i z_i e n_i^c \exp\left(-\frac{ez_i}{k_B T}(\psi - \psi_c)\right), \qquad (6)$$

where ε is the dielectric constant of the electrolyte, assumed to be uniform throughout). Integrate and apply symmetry at the channel's center ($d\psi/dy|_{y=d} = 0$) to obtain

$$\frac{d\psi}{dy} = +\left(2\frac{k_B T}{\varepsilon}\right)^{1/2} \left(\sum_i n_i^c \left[\exp\left(-\frac{ez_i}{k_B T}(\psi - \psi_c)\right) - 1\right]\right)^{1/2}. \qquad (7)$$

From this point onward in the derivation, the assumption is made that the background electrolyte is symmetric and binary ($z_+ =$

$-z_- = z$) to simplify the mathematical treatment, but the current model can be extended to include arbitrary electrolyte solutions.

For a symmetric, binary electrolyte Eq. (7) can be written as

$$\frac{d\psi}{dy} = \left(\frac{k_B T (2n_+^{well})}{\varepsilon}\right)^{1/2} (p^{1/2})\left\{2\sinh^2\left(\frac{ez}{2k_B T}(\psi - \psi_c)\right)\right.$$
$$\left. - \Omega \cdot \sinh\left(\frac{ez}{k_B T}(\psi - \psi_c)\right)\right\}^{1/2}, \qquad (8)$$

where

$$r^{well} \equiv n_-^{well}/n_+^{well},$$

$$p \equiv \exp\left(-\frac{ez}{k_B T}\psi_c\right) + r^{well} \exp\left(\frac{ez}{k_B T}\psi_c\right) = \frac{n_+^c + n_-^c}{n_+^{well}},$$

$$\Omega \equiv \frac{\exp(-\frac{ez}{k_B T}\psi_c) - r^{well}\exp(\frac{ez}{k_B T}\psi_c)}{\exp(-\frac{ez}{k_B T}\psi_c) + r^{well}\exp(\frac{ez}{k_B T}\psi_c)} = \frac{n_+^c - n_-^c}{n_+^c + n_-^c}. \qquad (9)$$

The second term within curly brackets in Eq. (8) ensures that equilibrium between the solution in the well and within the nanochannel is satisfied self-consistently. The parameter r^{well} is the ratio of volume-averaged negative to positive ion densities in the wells, it is typically very close to unity for nanochannels and relatively large wells, but it is kept here for consistency. A more detailed discussion of r^{well} is presented in Appendix A. The coefficient Ω measures free charge density at the centerline: $\Omega = 0$ for non-interacting EDLs, and $\Omega \to 1$ for strong overlap. p is the ratio of ionic strength of the channel centerline to that of the well. A more detailed discussion of p and Ω is given in Section 4. Here it is sufficient to note that for $r^{well} = 1$, $p = 2$ and $\Omega = 0$, one recovers the formulation of published models for thick, weakly-overlapped EDLs where the bulk ionic concentration in the middle of the channel is not significantly changed by the electric potential field [6,23]. Here this model is referred to as the "existing thick EDL model" [1,6–8, 10,30,31].

Up to this point in the derivation we have assumed that the potential distribution can be described using a planar, 1D geometry and symmetry with respect to the center plane, otherwise Eq. (8) is general and describes the potential distribution far from the ends of the channel. A second boundary condition is required to specify a unique solution for $\psi(y)$. Three boundary conditions reflect commonly accepted approximations of the behavior of electrolytes in contact with charged surfaces: specified wall-potential, specified surface charge density, or charge regulation [8,11,12,23, 32]. Consequences of each boundary condition are investigated. Of specific interest are conditions where the EDLs may be significantly overlapped.

2.2.1. Boundary condition I (BC I): specified wall-potential ($\psi(0) = \zeta$) [23]

Choosing $\tilde{\psi} \equiv ze(\psi - \psi_c)/k_B T$, $\tilde{\psi}_c \equiv ze\psi_c/k_B T$, $\lambda_D \equiv (\varepsilon k_B T/z^2 e^2(2n_+^{well}))^{1/2}$, and $\xi \equiv y/\lambda_D$, Eqs. (8) and (9) are recast in dimensionless form

$$\frac{d\tilde{\psi}}{d\xi} = (\tilde{p})^{1/2}\left\{2\sinh^2\left(\frac{\tilde{\psi}}{2}\right) - \tilde{\Omega} \cdot \sinh(\tilde{\psi})\right\}^{1/2}, \qquad (10)$$

$$\tilde{p} \equiv \exp(-\tilde{\psi}_c) + r^{well}\exp(\tilde{\psi}_c),$$

$$\tilde{\Omega} \equiv \frac{\exp(-\tilde{\psi}_c) - r^{well}\exp(\tilde{\psi}_c)}{\exp(-\tilde{\psi}_c) + r^{well}\exp(\tilde{\psi}_c)}. \qquad (11)$$

Here λ_D is a form of the Debye–Hückel thickness. The specified wall (shear plane) potential is the zeta potential, $\psi(0) = \zeta$, and the solution of Eq. (10) must satisfy $\tilde{\psi}_0 = \tilde{\psi}(0) = ze(\zeta - \psi_c)/k_B T$. Define zeta potential, ζ, as the potential at the shear plane measured relative to the well potential. The formal solution to Eq. (10)

is given by integrating from the wall to a position within the channel

$$\frac{y}{\lambda_D} = -\frac{1}{\tilde{p}^{1/2}} \int_{\tilde{\psi}}^{\tilde{\psi}_0} \left\{2\sinh^2\left(\frac{s}{2}\right) - \tilde{\Omega} \cdot \sinh(s)\right\}^{-1/2} ds. \qquad (12)$$

ψ_c is determined iteratively by numerically evaluating Eq. (12) at centerline where $y/\lambda_D = d/\lambda_D$ and $\tilde{\psi} = 0$ (see Appendix C for details about the numerical approximation of the integral in Eq. (13)):

$$\frac{d}{\lambda_D} = -\frac{1}{\tilde{p}^{1/2}} \int_0^{\tilde{\psi}_0} \left\{2\sinh^2\left(\frac{\tilde{\psi}}{2}\right) - \tilde{\Omega} \cdot \sinh(\tilde{\psi})\right\}^{-1/2} d\tilde{\psi}. \qquad (13)$$

Note that $\lambda_D/\sqrt{\tilde{p}}$ is now the effective Debye–Hückel thickness (relevant EDL thickness) in the presence of increased ion density in the channel. $\tilde{p}$ can be order 50 or larger (e.g., assuming a wall zeta potential of ~150 mV).

2.2.2. Boundary condition II (BC II): specified wall-charge density [23]

Again consider Eq. (8) (or the dimensionless form Eq. (10)) for a binary, symmetric electrolyte, but this time choose to specify the value of charge density at the wall

$$\sigma_E = -\varepsilon \frac{d\psi}{dy}\bigg|_{y=0}. \qquad (14)$$

From (10), the wall ($y = 0$)

$$\sigma_E^2 \left(\frac{ez}{\varepsilon k_B T}\right)^2 \frac{\lambda_D^2}{\tilde{p}} = 2\sinh^2\left(\frac{\tilde{\psi}_0}{2}\right) - \tilde{\Omega} \cdot \sinh(\tilde{\psi}_0). \qquad (15)$$

The parameter on the left-hand side of Eq. (15) measures $\sigma_E/((\varepsilon k_B T/ez)(\lambda_D/\sqrt{\tilde{p}}))$, the capacitance of the EDL across a thickness of order $\lambda_D/\sqrt{\tilde{p}}$, again the correction to the Debye–Hückel thickness in the presence of increased ion density in the channel. Note that both $\tilde{\psi}_0$ and $\tilde{\psi}_c$ are unknown at this stage of the formulation. To obtain a specific solution the coupled system Eqs. (12) and (13) is solved subject the constraint of Eq. (15).

2.2.3. Boundary condition III (BC III): charge regulation

Again consider Eq. (8) for a binary, symmetric electrolyte, and assume that there is an equilibrium reaction for the association and dissociation of silanol groups at the channel surface which depends on pH and ion concentration [11]. The assumptions implicit here are [11]:

(1) the deprotonation reaction at the fused silica surface is $SiOH \rightleftharpoons H_3O^+ + SiO^-$;
(2) counterions due to the charging of the surface (i.e., H_3O^+) provide a negligible contribution to the overall ionic strength of the solution;
(3) the surface potential is reduced linearly according to a basic Stern layer capacitance model [33].

The reaction kinetics yield the following relations between the potential and charge density near the wall and the potential in the bulk:

$$\zeta(\sigma_E) = \frac{k_B T}{e} \ln\frac{-\sigma_E}{e\Gamma + \sigma_E} - (pH - pK_a)\ln 10 \frac{k_B T}{e} - \frac{\sigma_E}{C}$$
$$\Rightarrow \tilde{\psi}_0$$
$$= -\tilde{\psi}_c + z\ln\frac{-\sigma_E}{e\Gamma + \sigma_E} - z(pH - pK_a)\ln 10 - \frac{ez}{k_B T}\frac{\sigma_E}{C}, \qquad (16)$$

where Γ is the fraction of chargeable sites that are dissociated, C is the Stern layer's phenomenological capacity [11], pH =

$-\log_{10}\{\gamma_{H_3O^+}[H_3O^+]\}$ and $pK_a = -\log_{10} K_a$ where K_a is the equilibrium constant of the surface deprotonation reaction. Here $\gamma_{H_3O^+}$ is the activity of the hydronium ion in solution [34]. As before, charge and surface potential are related according to

$$\sigma_E^2 \left(\frac{ez}{\varepsilon k_B T}\right)^2 \frac{\lambda_D^2}{\tilde{p}} = 2\sinh^2\left(\frac{\tilde{\psi}_0}{2}\right) - \tilde{\Omega} \cdot \sinh(\tilde{\psi}_0). \tag{17}$$

In this formulation, σ_E, $\tilde{\psi}_0$ and $\tilde{\psi}_c$ are unknown, and must be determined self-consistently. The formal solution of the differential equation (Eq. (8)) is still valid, and the solution requires satisfying the set of simultaneous equations Eqs. (12) and (13) subject to the constraints in (16)–(17).

2.3. Ionic mobility dependence on ionic strength and pH

At this stage the model for electric potential distribution across the channel depth has been defined, and three boundary conditions commonly used to find solutions for $\psi(y)$ have been described. In order to make predictions for measurable quantities, for example ionic current density, it is necessary to provide a framework for understanding the effect of an external field on liquid flow and ion transport. One important physical mechanism that is often overlooked in the micro- and nanofluidics community is the dependence of ionic mobility on local pH and ionic strength. This section presents a brief account to include such dependences. This issue is addressed in more detail in Part II of this two-paper series [35] where predictions of bulk solution conductivity and ionic current in nanochannels (with and without EDL overlap) are compared with experimental data.

The ionic mobility of any species varies with pH and ionic strength, (I_Z), of the electrolyte due to two known effects [34,36,37]. First, ionizable species exist in solution as an ensemble of ionic forms involved in fast (dynamic) association and dissociation reactions that determine the equilibrium (ensemble) form. Variations of local pH influence the effective ionic mobility by shifting the equilibrium condition for these reactions. For example, for a monovalent weak acid the equilibrium dissociation reaction and equilibrium constant are given by

$$HA \rightleftharpoons H_3O^+ + A^-, \tag{18}$$

$$K_a = \frac{\gamma_{A^-}\gamma_{H_3O^+}[H_3O^+][A^-]}{[HA]}, \tag{19}$$

where γ_j is the activity coefficient of species j (note that $\gamma_{HA} = 1$), and $[H_3O^+]$, $[A^-]$, $[HA]$ are the equilibrium concentrations of the hydronium ion, the conjugate base, and the undissociated weak acid, respectively. Continuing with this weak acid example and adopting the usual definitions of $pH = -\log_{10}\{\gamma_{H_3O^+}[H_3O^+]\}$ and $pK_a = -\log_{10} K_a$, the equilibrium constant can be expressed as

$$pK_a = pH - \log_{10}(\gamma_{A^-}) - \log_{10}\frac{[A^-]}{[HA]}. \tag{20}$$

A weak base will have a reaction of the form $BOH \rightleftharpoons B^+ + OH^-$, where $pK_b = -\log_{10} K_b$. Electrolytes with more complex ionic equilibria are common [34,38]. For now, simply note that, as explained below, ion mobility of any weak electrolyte is intimately coupled to the physics of the double layers (which partly determine ion density) and all reactions in the buffer. Equation (20) is one such coupling which is used here as an illustrative example.

Second, increase in ionic strength of a solution increases the effective electrostatic shielding of ions in solution and decreases their activity coefficients [37,39]. Ionic mobility decreases with increasing ionic strength. This effect can be described by a modified Debye–Hückel theory [34] result where finite ion size effects are included
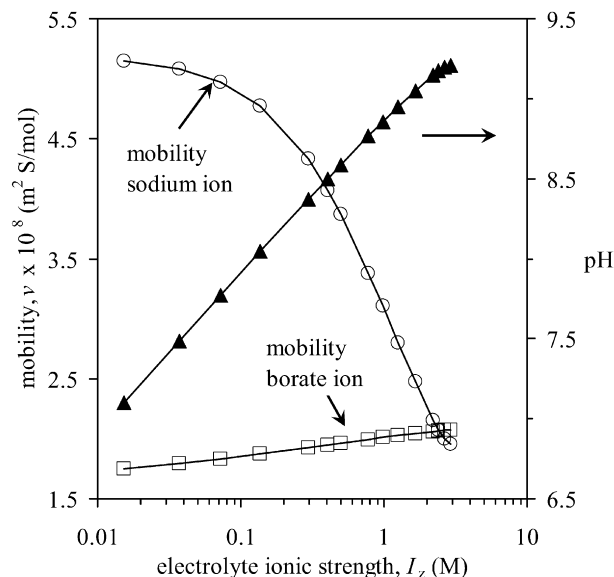

Fig. 2. Predicted values of bulk pH of sodium borate aqueous solution obtained dissolving borax salt in deionized water. Also shown are predicted electrophoretic mobilities of sodium ion (Na^+) and borate ion ($B(OH)_4^-$) as a function of electrolyte concentration. These predictions are based on the modified Debye–Hückel theory, Eqs. (22) and (23).

$$-\log_{10}(\gamma_{A^-}) = \frac{c_1 z\sqrt{I_Z}}{1 + c_2 a\sqrt{I_Z}}, \tag{21}$$

where $c_1 \approx 1.825(\varepsilon T)^{-3/2}$ and $c_2 \approx 50.3(\varepsilon T)^{-1/2}$ depend on the absolute temperature and the dielectric constant of the solvent ($c_1 \approx 0.508$ M$^{-1/2}$ and $c_2 \approx 0.329$ Å^{-1} M$^{-1/2}$ for water at 25 °C), $I_Z = 1/2 \sum_j z_j^2 c_j$ is the ionic strength, and a is an adjustable parameter related to the ion size (expressed in units of Å) [39].

The effective ionic mobility for a weak acid can be written as the product of the fraction of monovalent acid present in solution and its mobility at infinite dilution:

$$\nu_- = \frac{K_a}{[H_3O^+] + K_a}\nu_{-,\infty} = \frac{10^{-pK_a}}{10^{-pK_a} + 10^{-pH}}\nu_{-,\infty} \tag{22}$$

and, similarly, for a weak base

$$\nu_+ = \frac{[H^+]}{[H_3O^+] + K_a}\nu_{+,\infty} = \frac{10^{-pH}}{10^{-pK_a} + 10^{-pH}}\nu_{+,\infty}, \tag{23}$$

where $\nu_{\pm,\infty}$ are the mobilities at infinite-dilution, pK_a is given by Eqs. (20) and (21) (e.g., for the weak acid case). In experiments, background electrolyte concentrations of interest vary over several orders of magnitude (e.g., from tens of μM to hundreds of mM), resulting in large changes in pH and mobility.

As mentioned above, in Part II of this series a detailed model is developed for a realistic buffer of interest and the accuracy of these predictions is also discussed [35]. The model effectively gives a functional relationship between local pH and ion density for a borate buffer in contact with the atmosphere. The results of this model are summarized in Fig. 2 which shows sodium ion mobility and solution pH for a sodium borate solution in equilibrium with typical atmospheric CO_2 levels. Predictions are used here to make the point that even buffered solutions (e.g., borate buffer) cannot maintain a constant pH and mobility over ~4 orders of magnitude changes in concentration. The mobility of Na^+ is predicted to fall to ≈0.4 of its value at infinite-dilution (5.19×10^{-8} m^2 S/mol), and the mobility of $B(OH)_4^-$ is predicted to rise to 64% of its value at infinite dilution (3.29×10^{-8} m^2 S/mol). In the results presented in the next sections, realistic buffer mobility and pH values are incorporated in predicting ionic current in nanochannels (cf. Figs. 8 and 9).

Surprisingly, the effects of ion density and pH on mobility have not been widely incorporated into models of electrophoresis and current transport in either micro- or nanochannels. Nanochannels electrokinetic transport in particular is by definition strongly influenced by high ion density EDLs, and yet the author knows of no incorporation of ion density-dependent mobilities. Nanochannel studies which have assumed mobilities independent of ion density include those of Burgreen and Nakache [6], Hildreth [7], Pennathur and Santiago [3], Garcia et al. [2], Griffiths and Nilson [30], and others [8,19–22,32,40].

2.4. Electroosmotic flow

In this section, ion and bulk motion due to the application of an external field are discussed. The usual approximation is made that the electric potentials and ionic species distributions of the EDL remain unchanged as an external field is applied. This allows to treat the externally applied electric field (i.e., from well to well in Fig. 1) as a linearly superposable electric potential [6–8,30,41–45]. This is an assumption made here for simplification of the analysis, but that this is an issue that should be treated more carefully in future work. As discussed by Stone et al. [46,47] and Saville [48], for example, this "frozen EDL" assumption assumes we are interested in a regime characterized by $Pe = u_C d / \nu_C k_B T \ll 1$, where Pe is the electrophoretic Peclet number of ions, u_C is a characteristic speed of fluid motion, and ν_C is a characteristic ionic mobility. That is, it is assumed here that the transverse distribution of ions in the EDL is not affected by bulk motion. (Here advective current is accounted for through the contribution of bulk flow to axial ionic motion.) It is also assumed that the end-channel liquid wells are relatively large with negligible changes in ion density over time. Clearly, a fully coupled model where changes in the applied field can perturb charge distribution in and out of the nanochannel, and which takes into account end-effects, is complex and will perhaps be addressed in future work.

Electroosmotic flow is driven by the presence of net charge of the EDL. The unidirectional flow framework developed by Burgreen and Nakache [6] is applicable to electrokinetic flow in nanochannels with a high aspect ratio (width to depth), and when the flow is laminar (Re $\ll 1$). Under these conditions viscous flow is governed by

$$\mu \frac{d^2 u}{dy^2} - \frac{dp}{dx} - \rho_E E_x = 0, \tag{24}$$

where μ is the viscosity of the fluid, u is the fluid velocity in the axial direction, p is pressure, and E_x is the applied axial electric field. Expanding in terms of electroosmotic and pressure-driven flow components as $u = u_{EOF} + u_p$ and exploiting the linearity of the momentum balance we write

$$\frac{d^2 u_{EOF}}{dy^2} = -\frac{\varepsilon}{\mu} E_x \frac{d^2 \psi}{dy^2}; \qquad \frac{du_{EOF}}{dy} = \frac{d\psi}{dy} = 0 \quad \text{at } y = d,$$

$$u_{EOF} = 0, \qquad \psi = \zeta \quad \text{at } y = 0, \tag{25}$$

$$\frac{d^2 u_p}{dy^2} = \frac{1}{\mu} \frac{dp}{dx}; \qquad \frac{du_p}{dy} = 0 \quad \text{at } y = d,$$

$$u_p = 0 \quad \text{at } y = 0. \tag{26}$$

Further note that Eqs. (24) through (26) apply to regions of long-thin nanochannels away from interfaces. In such channels, EDL potential gradients that drive flow are solely in the y-direction as discussed in Appendix C.

Solving Eqs. (26) is straight forward when the pressure gradient is uniform along the channel. Integrating Eq. (26) once from $y = d$

to y, integrating the resultant differential equation from $y = 0$ (the wall) to y, and applying the no-slip boundary condition yields

$$u_p(y) = \frac{1}{2\mu} y(y - 2d) \frac{dp}{dx}. \tag{27}$$

The implications of pressure-driven fractionation methods were investigated recently by Griffiths and Nilson [30] and will not be discussed here. Instead here the focus is on electroosmotic flow. When the applied electric field is uniform along the channel, integrating Eq. (25) from the center-line toward the wall, applying the symmetry conditions at the channel center-line, and integrating once more from the wall toward the center of the channel yields

$$u_{EOF}(y) = -\frac{\varepsilon}{\mu} E_x \zeta \left(1 - \frac{\psi(y)}{\zeta} \right); \tag{28}$$

it follows that the depth averaged electroosmotic velocity is given by

$$\langle u_{EOF} \rangle = -\frac{\varepsilon}{\mu} E_x \zeta \left(1 - \frac{1}{d} \int_0^d \frac{\psi}{\zeta} \, dy \right). \tag{29}$$

The velocity profile in (28) depends on the choice of boundary condition at the wall (through ζ), the channel depth (through d, ψ_c), and the conditions in the well (as ψ_c depends on ψ_{well}).

2.5. Net ionic current

Current is carried by the motion of ions relative to the bulk neutral fluid (conduction) and by the ions advected by bulk fluid flow. (Away from end effects, net ionic current due to diffusion is negligible.) The net current density in a binary electrolyte is given by

$$
\begin{aligned}
i(y) &= i_+(y) - i_-(y) \\
&= (n_+ ezu - n_+ ez\nu_+ E_x) - (n_- ezu - n_- ez\nu_- E_x) \\
&= \rho_E(y) u(y) - K_0 E_x \left[\cosh\left(\frac{ez}{k_B T} (\psi - \psi_c) \right) \right. \\
&\quad \left. - \gamma \sinh\left(\frac{ez}{k_B T} (\psi - \psi_c) \right) \right],
\end{aligned} \tag{30}
$$

where

$$
\begin{aligned}
K_0 &\equiv n_+^{well} ez \left(\nu_+ \exp\left(-\frac{ez}{k_B T} \psi_c \right) + r^{well} \nu_- \exp\left(\frac{ez}{k_B T} \psi_c \right) \right), \\
\gamma &\equiv \frac{\nu_+ \exp(-\frac{ez}{k_B T} \psi_c) - r^{well} \nu_- \exp(\frac{ez}{k_B T} \psi_c)}{\nu_+ \exp(-\frac{ez}{k_B T} \psi_c) + r^{well} \nu_- \exp(\frac{ez}{k_B T} \psi_c)} = \frac{\nu_+ n_+^c - \nu_- n_-^c}{\nu_+ n_+^c + \nu_- n_-^c}.
\end{aligned} \tag{31}
$$

Here K_0 is the effective bulk conductivity of the electrolyte, and $\nu_{\pm}$ are the mobilities of the background electrolyte ions. To be exact $\nu_{\pm}$ are functions of the local ionic strength and pH of the solution. The depth-averaged net current density is

$$
\begin{aligned}
\langle i \rangle &= \frac{1}{d} \int_0^d i(y) \, dy \\
&= \frac{1}{d} \int_0^d \rho_E(y) u(y) \, dy - E_x \left[\frac{1}{d} \int_0^d K_0 \cosh\left(\frac{ez}{k_B T} (\psi - \psi_c) \right) dy \right. \\
&\quad \left. - \frac{1}{d} \int_0^d K_0 \gamma \sinh\left(\frac{ez}{k_B T} (\psi - \psi_c) \right) dy \right].
\end{aligned} \tag{32}
$$

In Eq. (32) $K_0(y)$ and $\gamma(y)$ are each functions of the local ionic strength since, as discussed earlier, ionic mobilities ($\nu_{\pm}$) vary with ionic strength. This makes evaluation of Eq. (32) complex as it requires to express $\nu_{\pm}$ as local functions of $\psi(y)$. All predictions shown in Parts I and II of this two-paper series were obtained using this full Eq. (32), including $\nu_{\pm}$ which vary with local pH and ion density (e.g., vary within the EDL). An obvious approximation for Eq. (32) is to assume that the mobility $\nu_{\pm}$ do not vary in the transverse direction (not a function of y), but are exclusively a function the area-averaged ionic strength; Eq. (32) would then simplify to

$$i(y) \approx \frac{1}{d} \int_0^d \rho_E(y) u(y)\, dy$$
$$- \langle K_0 \rangle E_x \left[\frac{1}{d} \int_0^d \cosh\left(\frac{ez}{k_B T}(\psi - \psi_c) \right) dy \right.$$
$$\left. - \langle \gamma \rangle \frac{1}{d} \int_0^d \sinh\left(\frac{ez}{k_B T}(\psi - \psi_c) \right) dy \right], \qquad (33)$$

where $\langle K_0 \rangle$ and $\langle \gamma \rangle$ are area-averaged quantities. Note that this approximation is fairly accurate for low ionic strength solutions. For example, for $c_{BGE} = 1$ mM (the conditions for Fig. 8 below), accounting for non-uniform ion mobilities reduces predicted current density by about 16% relative to the area-averaged mobility assumption shown in Eq. (33). In Part II it is shown that for high values of the well concentration the approximation given in Eq. (33) is not satisfactory.

The first term on the right-hand side of Eq. (32) reflects the advective component of the electric current density. The pressure-driven flow and electroosmotic flow components of the velocity field each contribute to this. The contribution due to pressure gradient is

$$\int_0^d \rho_E(y) u_p(y)\, dy = \frac{\varepsilon}{\mu} \zeta \frac{dp}{dx} \left[d - \int_0^d \frac{\psi}{\zeta}\, dy \right], \qquad (34)$$

where the value of ζ depends on the boundary condition chosen. The contribution due to electroosmotic flow is expressed conveniently in terms of integrals on the electric potential. From Eq. (8)

$$\frac{1}{d} \int_0^d \rho_E(y) u_{EOF}(y)\, dy$$
$$= n_+^{well} e \frac{\varepsilon E_x \zeta}{\mu} \frac{\lambda_D}{d} \frac{1}{\tilde{p}^{1/2}} \int_0^{\tilde{\psi}_0} \frac{e^{-\tilde{\psi}_c} e^{-s} - r^{well} e^{\tilde{\psi}_c} e^s}{\{2\sinh^2(\frac{s}{2}) - \tilde{\Omega} \cdot \sinh(s)\}^{1/2}}\, ds. \qquad (35)$$

In Section 4 predictions are shown of current density based these equations. Advective current is clearly a critical issue in overlapped EDL electroosmotic flow.

3. Parameter estimates in thin EDL regime: zeta potential, surface charge density, and fraction of chargeable sites

The aim of this section is to generate a unique, self-consistent set of values for zeta potential, surface charge density, and fraction of chargeable sites all of which give rise to the same observed flow and current at one condition: the thin EDL case. The thin-EDL regime is then the control from which to extrapolate overlapped EDL behavior using the various assumptions regarding the surface conditions. In this section, a summary is given of parameter values
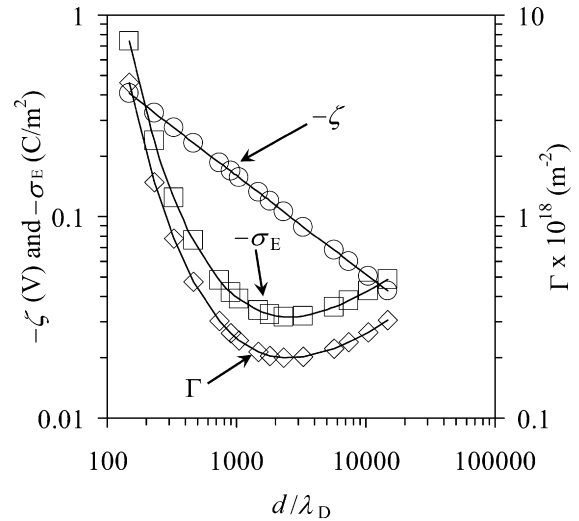

Fig. 3. Values of zeta potential (open circles) determined from current monitoring experiments in 20 μm deep channels, in conditions of thin EDLs [3]. Also shown are values of predicted surface charge density (open squares), and fraction of chargeable sites (Γ) (open diamonds), consistent with values of zeta potential determined experimentally.

that will be used in Section 4 to make predictions of observable quantities.

The starting point is to specify values of zeta potential determined experimentally via current monitoring [3] of electroosmotic flow in a 20 μm fused silica microchannel filled with a solution of sodium borate buffer in concentration that was varied between 1 and 100 mM. A convenient power law fit of the experimentally determined zeta potential as a function of the BGE concentration is shown in Fig. 3 with open circles, and was given by [3]

$$\zeta = -a \cdot c_{BGE}^b, \qquad (36)$$

where $a = 0.0288$, $b = -0.245$, c_{BGE} is the concentration (in molar units) of the BGE, and ζ is calculated in volts [3]. The assumption is made that Eq. (36) holds when making predictions at specified ζ potential (BC I). Strictly speaking Eq. (36) is valid only in the range of experimental concentrations studied (1–100 mM). Predictions are shown for concentrations outside the experimentally validated range, but these are mere extrapolations from Eq. (36).

Next, the value of surface charge density is determined, that is consistent with the value of ζ at a specific concentration of sodium borate. To do so $\sigma_E = -\varepsilon\, d\psi/dy|_{y=0}$ is calculated using Eq. (8) and the value of ζ given by Eq. (36). Finally, the fraction of chargeable sites, Γ, is determined which is consistent with ζ, the value of σ_E at the same conditions, and which satisfies Eq. (16), where the remaining parameters take the following values: $pK_a = 6.57$ and $C = 3.0$ F/m^2 [10,11]. The value of pH measured in the bulk (pH 8.25) is used in the calculation for Γ. In the thin EDL regime, bulk pH is an accurate estimate of the local pH in proximity of the surface [11].

In Fig. 3 computed values of σ_E and Γ are plotted, that are consistent with the given relation for ζ. The values of zeta potential, surface charge density and fraction of chargeable sites in Fig. 3 are used in the calculations in Section 4.

4. Theoretical results for constant BGE well concentration, and varying channel depth

In this section, model predictions are presented for fixed well ion concentration but variable channel depth. In the follow-up paper (Part II), predictions are presented for fixed depth and variable ion density. These two cases are presented separately because ion
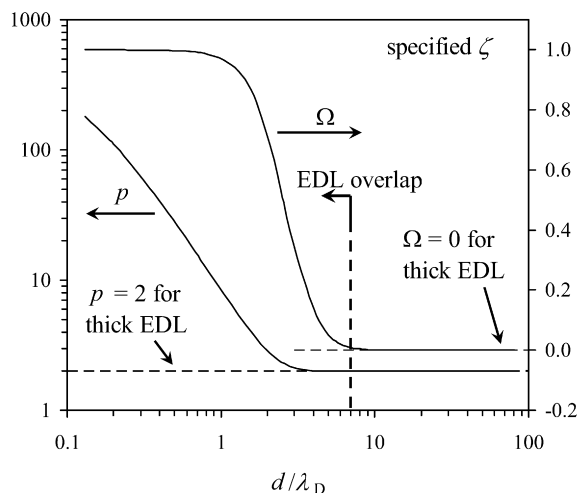
Fig. 4. Values of p and Ω, defined in Eq. (9), for varying degrees of EDL overlap. Shown are results for specified ζ (BC I). Choosing one of the other two boundary conditions discussed in this paper yields similar profiles of p and Ω (data not shown).
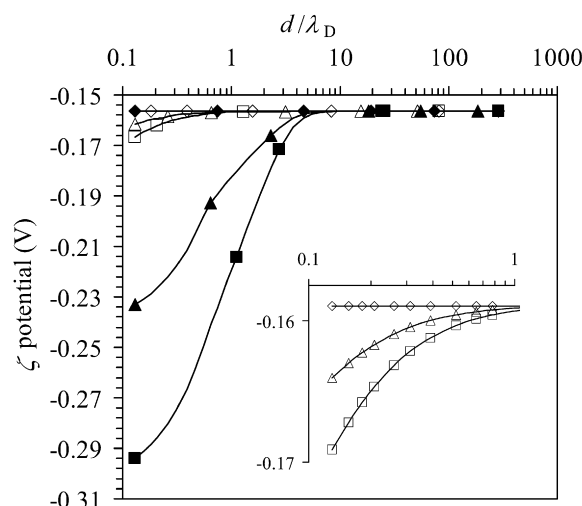

Fig. 5. Values of predicted electric potential at the shear plane (ζ) as a function of the ratio of the channel depth to the Debye thickness (d/λ_D). Results for the model described in Section 2 are shown with open symbols: specified ζ ($\diamond$); specified σ_E ($\square$); and charge regulation ($\triangle$). Results for the thick EDL model are shown with solid symbols: specified ζ ($\blacklozenge$); specified σ_E ($\blacksquare$); and charge regulation ($\blacktriangle$). Inset: predicted values of zeta potential in conditions of strong EDL overlap.

density in the wells directly affects zeta potential, ion mobility, pH, etc. Thus, results in this paper (Part I) are consistent with conditions (experiments) where the surface characteristics remain constant (specified well concentration). Results in Part II are representative of measurements where surface characteristics (zeta potential, surface charge, etc.) change due to changes in the concentration in the wells, at constant channel depth. Exploring both is useful as these are perhaps the two most important variables that can be controlled in experiments.

Channel depth is varied from the non-overlapped EDL regime to strong EDL overlap. Well concentration is fixed to 1 mM sodium borate (the background electrolyte, BGE). (See Section 4 in the second of Part II for a detailed description of the buffer.) This weak electrolyte is commonly used for buffering, has a relatively high pH 8.25, and a Debye length $\lambda_D \approx 9.6$ nm. The three boundary conditions presented in Section 2B reflect three assumptions regarding surface conditions. It is shown here that the model presented in this paper provides very consistent predictions independently of choice of boundary condition; on the other hand, different choices in boundary conditions lead to qualitatively different predictions when existing thick-EDL models are used.

In this section the aims are: (1) use the model of Section 2 to make predictions for nanochannels based on measured parameters in thin EDL regimes; (2) compare predictions obtained using the three boundary conditions discussed; and (3) compare model predictions to results obtained by the existing theory for thick EDLs [1,4–8,10,30,31]. To these aims values of the parameters (zeta potential, surface charge density, fraction of chargeable sites) are adopted that give consistent measurable quantities for all models in the thin EDL regime (as discussed in Section 3).

For strong degree of overlap, the EDL is predominantly made up of counter-ions, while co-ions are depleted from the channel. The functions p and Ω in Eq. (9) are summarized in Fig. 4 versus nondimensional channel depth for a specified ζ and $r^{well} = 1$. As EDLs overlap, n_+ becomes larger than n_-, and Ω saturates to its limiting value, $\Omega \to 1$. Similarly, p (describing centerline ion density relative to the well) increases with stronger overlap. Both parameters are strong functions of ψ_c and thus of the degree of overlap. In the thin-EDL regime, $d/\lambda_D \gg 1$, $\psi_c \approx 0$ so $\Omega \to 0$ and $p \to 2$, which agrees well with existing models. For stronger overlap, $d/\lambda_D < 7$, both p and Ω depart strongly from the thin-EDL limit and current models. Choosing an alternative boundary condition has negligible affect on p and Ω (plots not shown).

Next, predictions are presented based on the current model and are compared to existing thick EDL models. Values of zeta potential as a function of d/λ_D are plotted in Fig. 5. There are six theory curves. Focus first on predictions obtained using the model proposed here (open symbols). Results for specified ζ (BC I) obviously fall onto the horizontal line where $\zeta = -156$ mV (open diamonds). In BC II (fixed charge density and therefore fixed electric field at the wall) EDL overlap due to smaller channel depths implies larger values of ζ, ion density, and capacitive energy (open squares). EDL potential gradients are here "stronger," but in fact, for this range of channel depths, the increase in ζ is small. Predictions of ζ for BC II coincide with BC I ($\zeta = -156$ mV) for $d/\lambda_D > 1$ as expected (recall the choice of $\sigma_E = -39$ mC/m^2 corresponds to $\zeta = -156$ mV for the thin EDL limit). For $d/\lambda_D < 1$, the predicted zeta potential magnitude increases smoothly to a maximum of $\sim$1.07 times its thin EDL value at $d/\lambda_D = 0.13$. Predictions of zeta potential using the charge regulation boundary condition (BC III) are shown with open triangles. The predicted zeta potential at $d/\lambda_D = 0.13$ is $\sim$1.04 times its thin-EDL value. In BC III, the strength of the electric field at the shear plane is a function of the local pH and surface charge. Here, as channel depth decreases, local pH at the shear plane slightly decreases (to pH 8.1) but not enough to change Γ for this buffered, relatively high pH regime. This implies a decrease of σ_E (see Fig. 6) by only 10% and so the behavior is similar to BC II.

Now compare predictions using the proposed model to results from simulations using the existing thick EDL models described by Burgreen and Nakache [6] (see discussion in Section 1 and below Eqs. (8) and (9)). The results are shown in Fig. 5 with solid symbols. Predictions are shown that are based on this assumption and the three wall boundary conditions. For the "existing EDL" model, the centerline ion densities in the nanochannel are constrained to the specified value of 1 mM. This constraint directly affects the amount of surface net charge that can be shielded by counterions. At $d/\lambda_D = 0.46$ the predicted zeta potential for the existing model is approximately -259 mV (i.e., 1.7 times the thin EDL value). Furthermore, departure from thin EDL limit occurs at much larger channel depths ($d/\lambda_D \approx 7$) than for the proposed model. These results further highlight and exemplify the difference between predictions based on the proposed model and the classical thick EDL model. In the proposed model, counter-ions are recruited
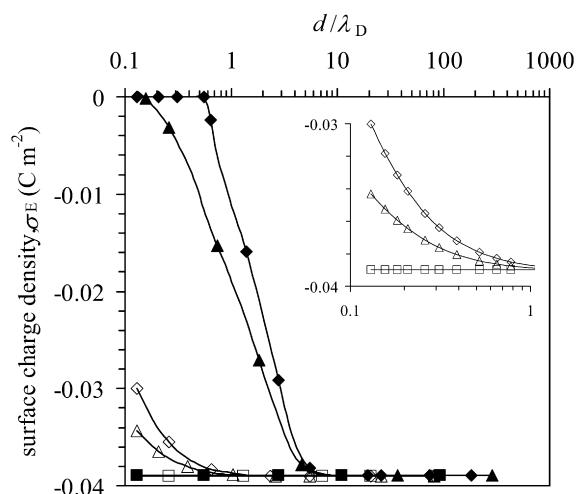
Fig. 6. Values of predicted surface charge density (σ_E) as a function of the ratio of the channel depth to the Debye thickness (d/λ_D). Results for the model described in Section 2 are shown with open symbols: specified ζ ($\Diamond$); specified σ_E ($\Box$); and charge regulation ($\triangle$). Results for the thick EDL model are shown with solid symbols: specified ζ ($\blacklozenge$); specified σ_E ($\blacksquare$); and charge regulation ($\blacktriangle$). Inset: predicted values of σ_E in conditions of strong EDL overlap.

Fig. 7. Predictions of area-averaged electroosmotic flow as a function of the ratio of the channel depth to the Debye thickness (d/λ_D), at constant BGE ion density ($c_{BGE} = 1$ mM). Results for the model described in Section 2 are shown with open symbols: specified ζ ($\Diamond$); specified σ_E ($\Box$); and charge regulation ($\triangle$). Results for the thick EDL model are shown with solid symbols: specified ζ ($\blacklozenge$); specified σ_E ($\blacksquare$); and charge regulation ($\blacktriangle$). Inset: predicted values of electroosmotic velocity in conditions of strong EDL overlap.
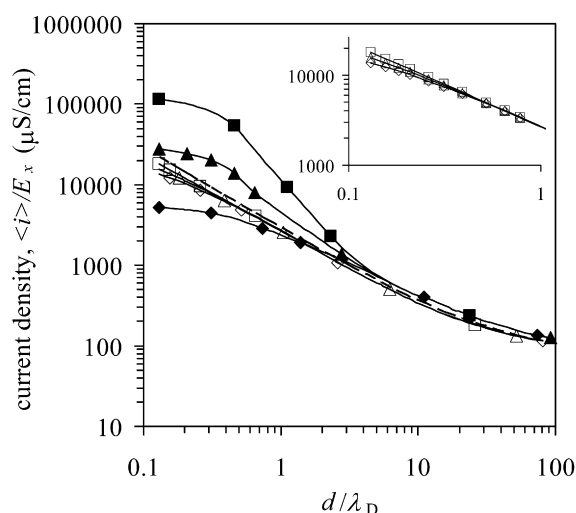
Fig. 8. Predictions of area-averaged ionic current density as a function of the ratio of the channel depth to the Debye thickness (d/λ_D), at constant BGE ion density ($c_{BGE} = 1$ mM). Results for the model described in Section 2 are shown with open symbols: specified ζ ($\Diamond$); specified σ_E ($\Box$); and charge regulation ($\triangle$). Results for the thick EDL model are shown with solid symbols: specified ζ ($\blacklozenge$); specified σ_E ($\blacksquare$); and charge regulation ($\blacktriangle$). Inset: predicted values of ionic current in conditions of strong EDL overlap. The dashed line is a plot of the estimated conductivity by Schoch et al., given in Eq. (37).

from the wells to satisfy axial equilibrium. This well-to-channel equilibrium requires an increase of free counter ion density in the nanochannel. The proposed model also calculates electric potential self-consistently to determine ψ_c and $n_\pm^c$. Similar trends are seen for the charge regulation boundary condition.

Predicted values of the surface charge density as a function of channel depth are shown in Fig. 6. Once again, focus first on the proposed model (open symbols). As expected, for $d/\lambda_D > 1$, σ_E is approximately -39 mC/m^2 for all three choices of boundary conditions (BCs I–III). For $d/\lambda_D < 1$, the electric field at the wall decreases, resulting in reduced surface charge density (except of course when σ_E is held constant). For comparison, also plotted in Fig. 6 are predictions based on existing thick EDL model (solid symbols). Again, it can be seen that specification of charge density at the centerline results in unphysically large deviations in predicted surface charge. Clearly the thick EDL model strongly overpredicts the differences between BCs I–III.

In Fig. 7 predictions are shown of area-averaged electroosmotic flow velocity (Eq. (29)) scaled by the Helmholtz–Smoluchowski velocity scale, $\langle u_{EOF} \rangle / \varepsilon E_x \zeta / \mu$. For $d/\lambda_D > 1$, $\langle u_{EOF} \rangle$ approaches u_{HS} as expected for all models. The proposed model predictions are shown with open symbols. Predictions of $\langle u_{EOF} \rangle$ are *nearly indistinguishable at all channel depths* studied, and for the three boundary conditions (BCs I–III). In strong EDL overlap conditions, electric potentials and observable quantities like area-averaged EOF are strongly influenced by the influx of counter-ions, as dictated by well-to-channel axial equilibrium. Predictions based on existing thick EDL theory (shown with solid symbols) are qualitatively different due to the (unphysical) constraint of fixed centerline ion densities relative to the well ion density.

The proposed model suggests that measurements made in thin EDL regime can be used to make unambiguous predictions of area-averaged EOF in nanochannels. This is important as it implies that there is nearly a one-to-one correlation between this observable quantity and the ion distributions in the channel (for fixed ion density in the wells).

Fig. 8 shows predicted values of area-averaged ionic current density (ratio of total current per area per electric field) as a function of d/λ_D. Again, predictions from the existing thick EDL model are shown as a comparison. The model proposed here shows consistent values, largely insensitive to the wall boundary conditions assumed. This is not the case for the existing thick EDL model
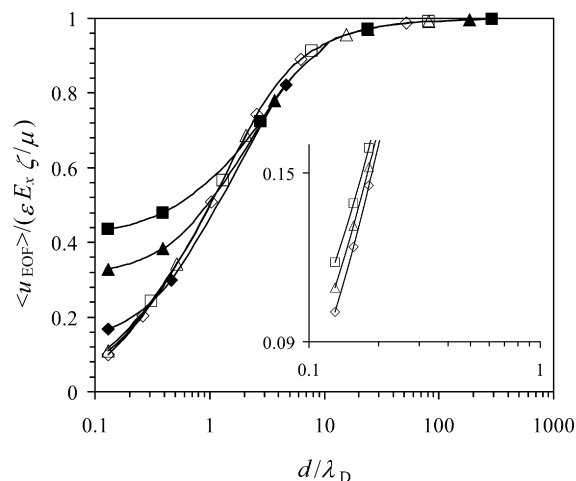
where, in conditions of overlap, predicted current density is a strong function of the surface condition. For the parameter range studied, current density for specified surface charge density can be almost two orders of magnitude larger than for specified zeta potential. This again has important consequences in reconciling experimental measurements and inferences on the physics in the nanochannel.

Predictions based on the model proposed here are in good agreement with the ad hoc expression for ionic current density proposed by Schoch et al. [4,5]. As mentioned in the introduction to this paper, Schoch et al. estimate conductivity as the sum of two terms: the expected bulk conductivity, and the conductivity of excess counterions due to the presence net surface charges. Their expression is written below expressed in units of conductivity:
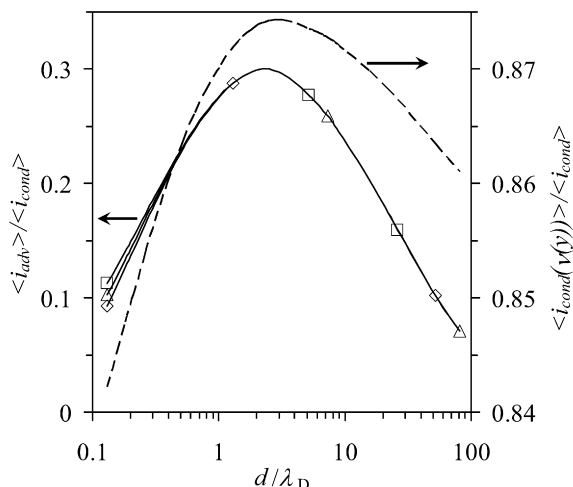
Fig. 9. Predicted values of the ratio of advective current to ionic conduction current as a function of the ratio of the channel depth to the Debye thickness (d/λ_D). Results for the model described in Section 2 are shown with open symbols: specified ζ ($\diamond$); specified σ_E ($\square$); and charge regulation ($\triangle$). Dashed-curve is the predicted ratio of advective current to ionic conduction current when variations in mobility are included (see Eq. (32)).

$$\frac{i}{E_x} = 10^3 (\nu_+ + \nu_-) c_{BGE} N_A e + (2\nu_+) \frac{\sigma_E}{2d}. \tag{37}$$

In Fig. 8, Eq. (37) is plotted with a dashed-curve, where σ_E is set to the value -53 mC/m^2 and d is varied. Equation (37) closely reproduces the simulated trends, and yields current density values which are consistent with simulations. An important reason for which this simple expression is successful is that advection current is only a small fraction of conduction even in strongly overlapped EDLs (Fig. 9). A second reason for this is that, at full well-to-channel equilibrium (and zeta potentials higher than the thermal voltage [23]), the shielding of wall charge (e.g., at high zeta potential) is mostly due the recruitment of counter ions from the well, while expulsion of co-ions is less important.

In Part II it is shown that Fig. 9 (left axis) is the relative contribution to current from advection and electromigration (again, for long thin channels where diffusive current is negligible). For large d/λ_D, current is dominated by electromigration of ions outside of the EDL (at well bulk conductivity). For $d/\lambda_D \approx 2.3$ and lower, two effects contribute to a rise in current density: increased ion density due to EDL and advection of charge due to electroosmosis. Again it is possible to see that the (slight) effects of the three model assumptions are confined to extreme conditions of overlap, $d/\lambda_D \sim 0.1$. Note there is an optimum at $d/\lambda_D \approx 2.3$. Advective currents are determined by the competition between the electroosmotic flow (which reduces in strength as the channel depth is decreased since $(\zeta - \psi_c) \to 0$), and free-charge density which increases due to overlap. Ion advection does not dominate Ohmic current for any of the cases studied here. For $d/\lambda_D < 2.3$, EOF contribution to total current become less important than the effect of increased conductivity (and associated Ohmic current) due to recruitment of counterions from the well. Finally, Fig. 9 is a plot of current density calculated using Eq. (32) divided by current density calculated using the less accurate Eq. (33). The effect of ionic strength on ionic current density measurements is described in detail in Part II. For now, note that the effect of the variation and non-uniformity of local ionic strength on mobility cannot be neglected in nanochannels. Predicted current density using values of mobilities at the channel centerline ion density (no y dependence) are consistently larger than those calculated using the correct values of local ionic strength (y dependence). Differences for the specific case studied here are between 12% and 16%. When the electrolyte concentration in the well is 1 mM (as in these calcula-

tions), we would expect ion mobilities to be approximately equal to their value for thin EDL conditions and infinite-dilution (Fig. 2). This is not the case for significant EDL overlap because the local ionic strength within the nanochannel is larger than in the wells. Ion mobility in nanochannels is reduced due to the increases in local ion density. That is, well-to-channel equilibrium dictates that ions in nanochannels should be relatively "slow."

Overall, the results of this section show that a self-consistent treatment of well-to-nanochannel electrochemical equilibrium yields result that are largely independent of the boundary conditions studied, over the range of interest here. For example, BCs II and III predict respective increases in zeta by 7% and 4%, relative to thin EDL value; while BC I predicts surface charge decrease by 10%. There is therefore an approximately one-to-one correlation between two important observable quantities (flow and current) and the ion distributions in the channel and wall. This consistency is important as it suggests that BCs I, II, and III are all useful in predicting nanochannel transport. The results also show that existing thick EDL models based on Burgreen and Nakache type formulations (which do not self consistently account for channel-to-well equilibrium) incorrectly predict strong differences in EOF and in ionic currents depending on choice of boundary condition.

5. Conclusions and recommendations

In this paper a physicochemical model is presented which self-consistently treats the electrochemical equilibrium between a channel and its connecting wells. The set of equations which is derived is new and it is used to form predictions for electric potential, electroosmotic flow, and ionic current in long, thin nanochannels. This model can be used to make predictions on nanochannel transport (including strongly overlapped EDLs) based on electrokinetic parameters measured in microchannels (i.e., thin EDL conditions). Predictions using this model are largely insensitive to the choice among the following three boundary conditions: specified zeta potential, specified surface charge density, and charge regulation. Model predictions have five important features. First, the theoretical description hinges on the fact that ion densities within nanochannels are not necessarily equal to those of the wells used to introduce the solution to the channels themselves. In fact nanochannel "bulk" concentrations (centerline concentrations) must be calculated self-consistently imposing equilibrium between solutions in the wells and within the nanochannel. The electrostatic potential field depends on three parameters: the ratio of ion density in the channel to ion density in the wells; the ratio of free-charge density to bulk ion density within the channel; and, a modified Debye–Hückel thickness ($\lambda_D/\sqrt{\bar{p}}$), which is the relevant scale for shielding of surface net charge. Second, the model shows ionic mobilities should be a strong function of concentration when the background electrolyte ionic strength is sufficiently large ($\gtrsim 1$ mM). Ionic mobilities must then be corrected to account for these differences (using for example an extended Debye–Hückel theory). Third, in conditions of strong EDL overlap, electroosmosis (bulk flow) contributes only a small fraction of the net ionic current; most of the observable current is due to conduction in conditions of increased counterion density. Fourth, the model yields guidelines for evaluating the strength and spatial extent of end effects including gradients of net charge, potential, and pressure. Fifth, the model shows that cross-section-area-averaged nanochannel charge (including wall charge) is not electrically neutral as axial fields are required for channel-to-well electrochemical equilibrium. Overall, the model shows that influx of counter ion concentration in the nanochannel (and, to a lesser degree, efflux of co-ions), contributes to improved screening of the wall charge and a lowering of ion mobility. This results in more moderate pre-

dictions of center line potential, electroosmotic flow, and current density relative to most models in the literature.

In the second of this two-paper series (Part II), the effect of local ionic strength and pH on ion mobility is explored in detail, and an experimental validation of the model is provided.

Appendix A

Overall, global net neutrality for the system implies that free net charge in the channel and wells balances all wall charges:

$$
\begin{aligned}
z_f S^{\mathrm{ch}} \sigma_{\mathrm{E}} &= e \sum_i z_i \big(N_i^{\mathrm{well}} + N_i\big) \\
&= z e n_+^{\mathrm{well}} \big(2 V^{\mathrm{well}}\big) \Bigg\{ 1 + \frac{1}{d} \frac{V^{\mathrm{ch}}}{V^{\mathrm{well}}} \exp\left(-\frac{ez}{k_{\mathrm{B}}T}\psi_{\mathrm{c}}\right) \\
&\quad \times \int_0^d \exp\left(-\frac{ez}{k_{\mathrm{B}}T}(\psi - \psi_{\mathrm{c}})\right) dy \\
&\quad - 1 - \frac{1}{d} \frac{V^{\mathrm{ch}}}{V^{\mathrm{well}}} r^{\mathrm{well}} \exp\left(\frac{ez}{k_{\mathrm{B}}T}\psi_{\mathrm{c}}\right) \\
&\quad \times \int_0^d \exp\left(\frac{ez}{k_{\mathrm{B}}T}(\psi - \psi_{\mathrm{c}})\right) dy \Bigg\},
\end{aligned}
\tag{A.1}
$$

here, for simplicity, it is assumed that well walls are neutral, but this assumption does not qualitatively change the formulation, where S^{ch} and V^{ch} are the surface area and volume of the channel, respectively, V^{well} is the volume of one of two identical wells, N_i is the number of free charges in solution within the channel, and N_i^{well} is the number of free charges in the wells. Equation (A.1) can be rewritten as

$$
r^{\mathrm{well}} = \frac{1 + \frac{1}{d}\frac{V^{\mathrm{ch}}}{V^{\mathrm{well}}} \exp(-\frac{ez}{k_{\mathrm{B}}T}\psi_{\mathrm{c}}) \int_0^d \exp(-\frac{ez}{k_{\mathrm{B}}T}(\psi - \psi_{\mathrm{c}}))\, dy}{1 + \frac{1}{d}\frac{V^{\mathrm{ch}}}{V^{\mathrm{well}}} \exp(\frac{ez}{k_{\mathrm{B}}T}\psi_{\mathrm{c}}) \int_0^d \exp(\frac{ez}{k_{\mathrm{B}}T}(\psi - \psi_{\mathrm{c}}))\, dy} \\
- \frac{\frac{S^{\mathrm{ch}}}{2V^{\mathrm{well}}}\frac{z_f \sigma_{\mathrm{E}}}{zen_+^{\mathrm{well}}}}{1 + \frac{1}{d}\frac{V^{\mathrm{ch}}}{V^{\mathrm{well}}} \exp(\frac{ez}{k_{\mathrm{B}}T}\psi_{\mathrm{c}}) \int_0^d \exp(\frac{ez}{k_{\mathrm{B}}T}(\psi - \psi_{\mathrm{c}}))\, dy}.
\tag{A.2}
$$

where r^{well} is a function of the electric potential at the centerline, the bulk ion concentration in the wells, the surface charge density at the channel walls, and of the relative sizes of the channel and the wells. In fact, when the number of electrolyte ions is large compared to the number of net wall charges ($z_f S^{\mathrm{well}} \sigma_{\mathrm{E}} \ll zen_+^{\mathrm{well}} V^{\mathrm{well}}$), and EDLs are not overlapped ($\psi_{\mathrm{c}} \approx 0$): $r^{\mathrm{well}} \approx 1$, $p = 2$ and $\Omega = 0$. Otherwise, when EDLs overlap

$$
r^{\mathrm{well}} \approx \frac{1 + \frac{1}{d}\frac{V^{\mathrm{ch}}}{V^{\mathrm{well}}} \exp(-\frac{ez}{k_{\mathrm{B}}T}\psi_{\mathrm{c}}) \int_0^d \exp(-\frac{ez}{k_{\mathrm{B}}T}(\psi - \psi_{\mathrm{c}}))\, dy}{1 + \frac{1}{d}\frac{V^{\mathrm{ch}}}{V^{\mathrm{well}}} \exp(\frac{ez}{k_{\mathrm{B}}T}\psi_{\mathrm{c}}) \int_0^d \exp(\frac{ez}{k_{\mathrm{B}}T}(\psi - \psi_{\mathrm{c}}))\, dy} > 1.
\tag{A.3}
$$

Equation (A.2) is a more accurate and general constraint than the two separate conditions applied by Conlisk et al. [20,21]. In experiments r^{well} is nearly identical to unity (as adopted by Conlisk et al.). However, r^{well} is different than unity because of the required electro-chemical equilibrium between the nanochannel and the well. Physically there must be a net deficit of counter charge in the well to (and near the nanochannel inlet or outlet) to maintain the potential difference $\psi^{\mathrm{well}} - \psi(x)$. For large wells and shallow channels, $r^{\mathrm{well}} \sim 1$ is a very good approximation for estimating observable quantities, which we will adopt. However, Eq. (A.2) is useful as a strict constraint and reminder that channel-well equilibrium requires that r^{well} not be identically equal to unity.

Appendix B

Sections 2.1–2.5 established that chemical equilibrium between a nanochannel and end-channel wells implies nonzero, axial ion and potential gradients. For simplicity, the assumption was made of long, thin channel regions away from inlets/outlets in estimating net bulk and ion flow integrals. A fair question is: How far inside the channel do such gradients persist? In fact, end effects are important inside the channel only for axial distances on the order of the Debye length. An exact expression for this distance x_{d} is given below:

$$
\begin{aligned}
\frac{x_{\mathrm{d}}}{\lambda_{\mathrm{D}}} &= \frac{2e^{\tilde{\psi}_{\mathrm{c}}/2}}{(e^{-\tilde{\psi}_{\mathrm{c}}} + r^{\mathrm{well}} e^{\tilde{\psi}_{\mathrm{c}}})^{1/2}} \left(\frac{-1 + e^{-\tilde{\psi}_{\mathrm{c}}}}{1 - e^{\tilde{\psi}_{\mathrm{c}}}}\right)^{1/2} \\
&\quad \times \ln\big[e^{-\tilde{\psi}_{\mathrm{c}}/2} + (-1 + e^{-\tilde{\psi}_{\mathrm{c}}})^{1/2}\big].
\end{aligned}
\tag{B.1}
$$

This expression is derived by first integrating the axial component of the Poisson equation along the centerline from x_{d} (a location far into the channel where $\partial\psi/\partial x|_{x_{\mathrm{d}}} = 0$) to a position x in the direction of the well ($0 \leqslant x \leqslant x_{\mathrm{d}}$, see Fig. 1). Then integrate a second time along the centerline from $x = 0$ where $\psi(x = 0) = \psi_{\mathrm{well}} \equiv 0$ to x_{d}. Fig. 10 is a plot of the (dimensionless) axial distance over which the electric potential reaches its value at the centerline as a function of d/λ_{D}, at a fixed ion concentrations in the wells, for the three boundary conditions described. The curve shows that at most the axial distance x_{d} is slightly larger than the Debye length, λ_{D}. A maximum occurs near $d/\lambda_{\mathrm{D}} \approx 1$, where $x_{\mathrm{d}}/\lambda_{\mathrm{D}} \approx 1.3$. For $d/\lambda_{\mathrm{D}} > 1$, x_{d} decreases because the potential at the centerline, ψ_{c}, decays to zero as channel depth increases. The strong overlap ($d/\lambda_{\mathrm{D}} < 1$) regime is characterized by weak shielding of surface charges, and by large (negative) values of the transverse electric potential at the center-line. Large ψ_{c} therefore strongly affect the axial electric field and can also impose a short axial length scale over which transverse equilibrium is attained. Note assumptions regarding the wall boundary conditions do not significantly affect x_{d}.

At equilibrium, liquid velocity is zero everywhere, $\mathbf{u} = 0$. Therefore, there exists an axial osmotic pressure gradient that balances the axial variation of electric potential from ψ_{well} to ψ_{c} along the centerline. As already discussed, variation occurs over a length
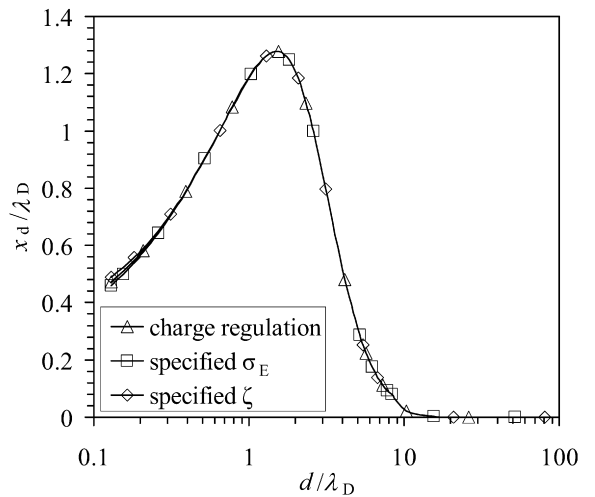
Fig. 10. Dimensionless axial distance ($x_{\mathrm{d}}/\lambda_{\mathrm{D}}$) over which the electric potential reaches its value at the centerline of the nanochannel (ψ_{c}) as a function of the ratio of the channel depth to the Debye thickness (d/λ_{D}) at a fixed BGE concentration (1 mM).

scale on the order of the Debye length. For a binary, symmetric electrolyte, the equilibrium pressure distribution is given by

$$\frac{\partial p}{\partial x} = \rho_E \frac{\partial \psi}{\partial x} = \left[e \sum_i z_i n_i^{\text{well}} \exp\left(-\frac{ez_i}{k_B T} \psi(x) \right) \right] \frac{\partial \psi}{\partial x} \qquad \text{(B.2)}$$

so that

$$\begin{aligned}
p(x, y = d) &= \int_0^{\psi_c} \left[e \sum_i z_i n_i^{\text{well}} \exp\left(-\frac{ez_i}{k_B T} \psi_c \right) \right. \\
&\quad \left. \times \exp\left(-\frac{ez_i}{k_B T} (\psi - \psi_c) \right) \right] d\psi \\
&= k_B T n_+^{\text{well}} \left\{ 1 + r^{\text{well}} - \left[\exp\left(-\frac{ez}{k_B T} \psi_c \right) \right. \right. \\
&\quad \left. \left. + r^{\text{well}} \exp\left(\frac{ez}{k_B T} \psi_c \right) \right] \right\}.
\end{aligned} \qquad \text{(B.3)}$$

The pressure distribution (B.1) does not cause liquid flow. As we have seen, flow is achievable in the presence of an externally applied axial electric field (electroosmotic flow) or in the presence of a net pressure difference between channel wells. For a channel of uniform cross section and wells with equal ion density, $p(x, y)$ is symmetric along x and so exerts no net axial force on the liquid in the nanochannel.

Lastly, an expression is presented for area-averaged "net" charge near the end of the nanochannel, where (fixed) wall charge is added to charge in the bulk of the channel:

$$\begin{aligned}
&2\sigma_E(2d + w) + \rho_E(2dw) \\
&= 2\sigma_E(2d + w) + (2dw)\left(ezn_+^{\text{well}} \right) \\
&\quad \times \left[\exp\left(-\frac{ez}{k_B T} \psi(x) \right) - \exp\left(\frac{ez}{k_B T} \psi(x) \right) \right].
\end{aligned} \qquad \text{(B.4)}$$

The expression shows that the sum of charge along the channel cross section (including the wall), $2\sigma_E(2d + w) + \rho_E(2dw)$, is not necessarily zero as been assumed by previous models [17,19–22, 49]. Area-averaged charge (including wall) is zero only for regions far from the inlet.

Appendix C

Note the integrand in Eq. (13) has an integrable singularity when $\tilde{\psi} = 0$. To evaluate the integral numerically we divide the integration range into $[0, \tilde{\psi}_w] = [0, \varepsilon_{\tilde{\psi}}] + [\varepsilon_{\tilde{\psi}}, \tilde{\psi}_w]$, where $|\varepsilon_{\tilde{\psi}}| \ll 1$, and expand the integrand about $\varepsilon_{\tilde{\psi}}$ to obtain an approximate expression for the integral close to the point $\tilde{\psi} = 0$:

$$\begin{aligned}
&\int_0^{\varepsilon_{\tilde{\psi}}} \left\{ 2\sinh^2\left(\frac{\tilde{\psi}}{2} \right) - \tilde{\Omega} \cdot \sinh(\tilde{\psi}) \right\}^{-1/2} d\tilde{\psi} \\
&\approx 2\left(-\frac{\varepsilon_{\tilde{\psi}}}{\tilde{\Omega}} \right)^{1/2} + \frac{1}{6}\left(-\frac{\varepsilon_{\tilde{\psi}}}{\tilde{\Omega}} \right)^{3/2} + O\left[\left(-\frac{\varepsilon_{\tilde{\psi}}}{\tilde{\Omega}} \right)^{5/2} \right].
\end{aligned} \qquad \text{(C.1)}$$

References

[1] D. Stein, M. Kruithof, C. Dekker, Phys. Rev. Lett. 93 (3) (2004) 035901.
[2] A.L. Garcia, L.K. Ista, D.N. Petsev, M.J. O'Brien, P. Bisong, A.A. Mammoli, S.R.J. Brueck, G.P. Lopez, Lab Chip 5 (11) (2005) 1271–1276.
[3] S. Pennathur, J.G. Santiago, Anal. Chem. 77 (21) (2005) 6782–6789.
[4] R.B. Schoch, P. Renaud, Appl. Phys. Lett. 86 (25) (2005) 253111.
[5] R.B. Schoch, H. van Lintel, P. Renaud, Phys. Fluids 17 (10) (2005) 100604.
[6] D. Burgreen, F.R. Nakache, J. Phys. Chem. 68 (5) (1964) 1084–1091.
[7] D. Hildreth, J. Phys. Chem. 74 (9) (1970) 2006–2015.
[8] S. Levine, J.R. Marriott, K. Robinson, J. Chem. Soc. Faraday Trans. II 71 (1) (1975) 1–11.
[9] Qualitatively similar results were obtained by Karnik et al. [31] who found that values of the surface net charge density between −2 and −100 mC/m^2 adequately fit their experimental results in long, thin 35 nm deep silicon dioxide channels.
[10] F.H.J. van der Heyden, D. Stein, C. Dekker, Phys. Rev. Lett. 95 (11) (2005) 116104.
[11] S.H. Behrens, D.G. Grier, J. Chem. Phys. 115 (14) (2001) 6716–6721.
[12] B.W. Ninham, V.A. Parsegian, J. Theor. Biol. 31 (3) (1971) 405–428.
[13] D.E. Yates, S. Levine, T.W. Healy, J. Chem. Soc. Faraday Trans. I 70 (1974) 1807–1818.
[14] W. Qu, D. Li, J. Colloid Interface Sci. 224 (2) (2000) 397–407.
[15] C.L. Ren, Y.D. Hu, D.Q. Li, C. Werner, J. Adhes. 80 (9) (2004) 831–849.
[16] T.W. Healy, L.R. White, Adv. Colloid Interface Sci. 9 (4) (1978) 303–345.
[17] H.S. Kwak, E.F. Hasselbrink, J. Colloid Interface Sci. 284 (2) (2005) 753–758.
[18] S. Kang, Y.K. Suh, J. Mechan. Sci. Technol. 20 (12) (2006) 2250–2264.
[19] A.T. Conlisk, J. McFerran, Z. Zheng, D. Hansford, Anal. Chem. 74 (9) (2002) 2139–2150.
[20] Z. Zheng, D.J. Hansford, A.T. Conlisk, Electrophoresis 24 (17) (2003) 3006–3017.
[21] S. Bhattacharyya, Z. Zheng, A.T. Conlisk, J. Fluid Mech. 540 (2005) 247–267.
[22] F. Tessier, G.W. Slater, Electrophoresis 27 (3) (2006) 686–693.
[23] R. Hunter, Zeta Potential in Colloid Science Principles and Applications, Academic Press, London, 1981.
[24] S. Pennathur, J.G. Santiago, Anal. Chem. 78 (3) (2006) 972.
[25] A. Hibara, T. Saito, H.B. Kim, M. Tokeshi, T. Ooi, M. Nakao, T. Kitamori, Anal. Chem. 74 (24) (2002) 6170–6176.
[26] S.R. Liu, Q.S. Pu, L. Gao, C. Korzeniewski, C. Matzke, Nano Lett. 5 (7) (2005) 1389–1393.
[27] A. Plecis, R.B. Schoch, P. Renaud, Nano Lett. 5 (6) (2005) 1147–1155.
[28] Y.C. Wang, A.L. Stevens, J.Y. Han, Anal. Chem. 77 (14) (2005) 4293–4299.
[29] D. Mijatovic, J.C.T. Eijkel, A. van den Berg, Lab Chip 5 (5) (2005) 492–500.
[30] S.K. Griffiths, R.H. Nilson, Anal. Chem. 78 (23) (2006) 8134–8141.
[31] R. Karnik, R. Fan, M. Yue, D.Y. Li, P.D. Yang, A. Majumdar, Nano Lett. 5 (5) (2005) 943–948.
[32] S. Levine, J.R. Marriott, G. Neale, N. Epstein, J. Colloid Interface Sci. 52 (1) (1975) 136–149.
[33] R.F. Probstein, Physicochemical Hydrodynamics: An Introduction, second ed., Wiley, New York, 1994.
[34] D.A. Skoog, D.M. West, F.J. Holler, S.R. Crouch, Fundamentals of Analytical Chemistry, eighth ed., Brooks Cole, Belmont, USA, 2003.
[35] F. Baldessari, J. Colloid Interface Sci. (2008), doi:10.1016/j.jcis.2008.06.008.
[36] W. Friedl, J.C. Reijenga, E. Kenndler, J. Chromatogr. A 709 (1) (1995) 163–170.
[37] P. Bocek, M. Deml, P. Gebauer, V. Dolnik, Analytical Isotachophoresis, VCH, New York, 1988.
[38] For example, sodium borate solutions typically involve two equilibrium reactions with six species in solution: sodium ion, tetraborate ion, borate ion, buric acid, hydroxyl ion, and hydronium ion. This equilibrium can also be affected by interaction of the solution with carbon dioxide in the atmosphere (which reacts with water to form carbonic acid). Sodium borate solutions is analyzed as an example "real electrolyte" in Part II of this two-paper series [35].
[39] P.G. Righetti, C. Gelfi, M.R. D'Acunto, Electrophoresis 23 (10) (2002) 1361–1374.
[40] S. Pennathur, J.G. Santiago, Anal. Chem. 77 (21) (2005) 6772–6781.
[41] T.M. Squires, S.R. Quake, Rev. Mod. Phys. 77 (3) (2005) 977–1026.
[42] S.K. Griffiths, R.H. Nilson, Anal. Chem. 72 (21) (2000) 5473–5482.
[43] S.K. Griffiths, R.H. Nilson, Anal. Chem. 72 (20) (2000) 4767–4777.
[44] S.K. Griffiths, R.H. Nilson, Anal. Chem. 71 (24) (1999) 5522–5529.
[45] E.B. Cummings, S.K. Griffiths, R.H. Nilson, P.H. Paul, Anal. Chem. 72 (11) (2000) 2526–2532.
[46] S.Y. Park, C.J. Russo, D. Branton, H.A. Stone, J. Colloid Interface Sci. 297 (2) (2006) 832–839.
[47] J.D. Sherwood, H.A. Stone, Phys. Fluids 7 (4) (1995) 697–705.
[48] R.A. Mosher, D.A. Saville, W. Thormann, The Dynamics of Electrophoresis, VCH, Weinheim, 1991.
[49] C. Myung-Suk, H.W. Kwak, Korea–Australia Rheol. J. 15 (2) (2003) 83–90.